Search for Anisotropies of cosmic ray electrons using LHAASO-WCDA

Dongxu Sun,[a,b,*] **Wei Liu,**[c,d] **Dan Li,**[c,d] **Qiang Yuan,**[a,b] **Hongbo Hu**[c,d] **and Yiqing Guo**[c,d] **for the LHAASO collaboration**

[a]*Key Laboratory of Dark Matter and Space Astronomy, Purple Mountain Observatory, Chinese Academy of Sciences, Nanjing 210023, China*

[b]*School of Astronomy and Space Science, University of Science and Technology of China, Hefei 230026, China*

[c]*Key Laboratory of Particle Astrophysics, Institute of High Energy Physics, Chinese Academy of Sciences, Beijing 100049, China*

[d]*University of Chinese Academy of Sciences, Beijing 100049, China*

E-mail: sundx@pmo.ac.cn, liuwei@ihep.ac.cn, lidan@ihep.ac.cn

Anisotropies of Cosmic Ray Electrons (CREs) above TeV energies are ideal probe of nearby electron accelerators due to the short propagation length of high-energy CREs. The Water Cherenkov Detector Array (WCDA) of the Large High Altitude Air Shower Observatory (LHAASO) is a survey type detector for cosmic rays and gamma rays above ∼ 100 GeV with a large field-of-view and a high duty cycle. The strong gamma/hadron separation capability and the large effective area of the WCDA make it a powerful detector of CREs whose fluxes are more than 1000 times lower than nuclei. Using 2 years of data collected by the WCDA with energies from several hundred GeV to tens of TeV, we search for possible anisotropies of CREs. The cosmic ray background in the CRE sample is studied carefully with simulations and the gamma-ray observations of crab nebula.

38th International Cosmic Ray Conference (ICRC2023)
26 July - 3 August, 2023
Nagoya, Japan

ICRC2023
38th International Cosmic Ray Conference
The Astroparticle Physics Conference

*Speaker

1. Introduction

Cosmic Rays (CRs) are high-energy particles accelerated by energetic sources such as shocks of supernova remnants (SNRs) or jets of black holes. After being accelerated, they propagate in the interstellar or intergalactic space and interact with materials and fields. Precise measurements of the energy spectra and anisotropies are the key to understanding the origin, acceleration, and propagations of CRs.

Non-trivial spectral structures of CR nuclei have been revealed by recent direct detection experiments ([4, 5, 7, 18, 19, 22]). Particularly, the hardenings around hundreds of GV and the subsequent softenings around 10 TV challenge the conventional acceleration and propagation model of CRs. Together with the energy evolution of large-scale anisotropies, a nearby source model was proposed to account for the spectral and anisotropy features simultaneously ([15, 20]).

The implied nearby source(s) may also leave imprints on the spectra of CR electrons and/or positrons (CREs) ([8, 11, 17, 21]). Particularly, supposing that the nearby source was an SNR with a pulsar left after the supernova explosion, the pulsar may explain the positron excess via accelerating $e^{\pm}$ pairs and the SNR may explain the spectral features of CREs and nuclei via accelerating primary particles ([12, 13]). Anisotropies of CREs could provide important tests of such a scenario. **Figure 1** shows the contributions to the CRE spectra by two sources as an illustration, Geminga with an age of ∼ 345 kyr and Vela with an age of 11.2 kyr, as well as the expected dipole anisotropy amplitude from them [16].
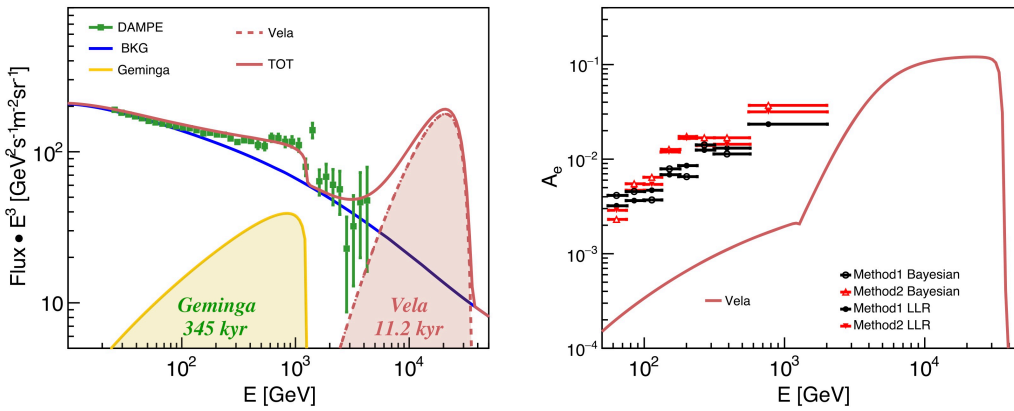
Figure 1: Left: Predicted CRE fluxes from Geminga, Vela, and the ensemble of a large number of background sources, compared with the DAMPE data [10]. Right: Predicted anisotropy amplitude contributed by Geminga and Vela, compared with the upper limits set by Fermi-LAT [1]. Figure from [16].

So far the only experiment that studied the cosmic-ray electron anisotropy in the GeV-TeV energy range is Fermi/LAT. The first observation of anisotropy of CREs is reported by Fermi-LAT in 2010, The upper limits for a dipole anisotropy ranged from 0.5% to 10% from 60 GeV up to 480 GeV. Latest results of Fermi-LAT places an upper limit on the dipole anisotropy of CREs between 42 GeV and 2 TeV at a 95% confidence level, ranging from 3×10^{-3} to 3×10^{-2} [1, 3]. Measurements extending to higher energies with better sensitivity are thus very important in revealing or constraining the properties of nearby CRE sources.

2. LHAASO-WCDA detector

As a composite ground-based particle detector array locating at (29°21′27.6″ N, 100°08′19.6″ E), LHAASO employs multiple detection methods, including three detector arrays: the 1 km^2 extensive air shower array (KM2A) , the water Cherenkov detector array (WCDA), and the wide-field Cherenkov telescope array (WFCTA) [9]. The WCDA, which is utilized for this analysis, has a total area of 78,000 m^2, comprising 3,120 photomultiplier tube arrays divided into three sub-arrays as shown in the **Figure 2**. It records the Cherenkov light signals produced by secondary particles in water using photomultiplier tubes of different sizes.

The WCDA's advantages for observing electron anisotropy near the TeV energy range include its large effective area compared to space experiments, enabling the detection of more high-energy electron events. Its wide field of view is essential for detecting large-scale anisotropy, and its sensitivity to electromagnetic showers allows for good direction sensitivity. The sensitive detection range of WCDA, from 100 GeV to 30 TeV, covers the TeV energy range of interest for studying electron anisotropy. Additionally, WCDA has strong gamma/proton discrimination capability, as it is highly sensitive to secondary cores in air showers and can construct multiple parameters to eliminate background noise [6].
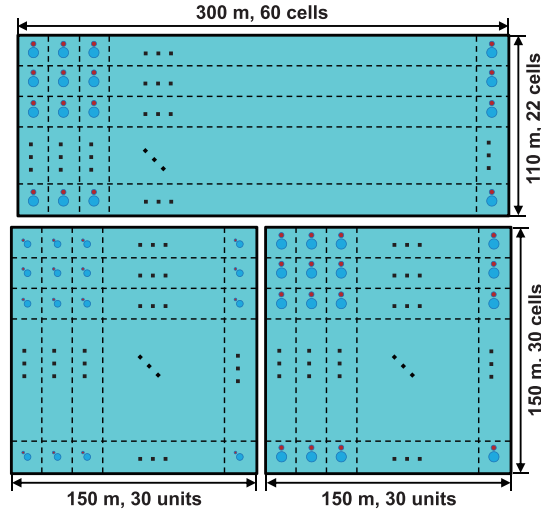
Figure 2: Schematic plot of the WCDA layout. The lower two ponds are WCDA-1 and WCDA-2 from left to right, and the upper one is WCDA-3.

3. Data Selection

The analysis presented in this study employed near two years (726 days) of WCDA data from April 2021 to March 2023. We have applied certain selection criteria in order to obtain reconstructed data that is collected under the optimal operational conditions of the WCDA. Thus some days which are gapped have the consideration of reconstruction quality. The event reconstruction method used in this study is based on the method described in this paper [6]. When an event is detected, the photomultiplier tube (PMT) emits photoelectrons (PEs), the number of which can range from 1 to

200,000. It utilizes the number of fired PMTs (N_{hit}) and have a time residual of less than 30ns or more than -30 ns, as well as a normalized charge exceeding 0.5 PEs. Primary energy distributions for gamma ray showers are estimated with simulation of shower to establish the correlation between the primary energy and N_{hit}. The result distribution in the seven bins of N_{hit} are plotted in **Figure 3**. Here, the median energy of the distributions used as the measure of the gamma ray energy for showers in the corresponding bins of N_{hit} are listed in the first two columns of Table 1.

Table 1: Summary of data used to analyse Crab. The PINCness cut is chosen by maximize the significance of Crab. The N_{evt} is the residual event number of CREs after PINCness cut. The residual ratio of cosmic ray and cosmic ray electrons is also shown.

N_{hit}	E_{med}/TeV	Significance	P	N_{evt}	R_{CR}	R_{CRE}
100-200	0.8	71.7	<1.085	13174.2	0.0127	0.567
200-300	1.6	101.3	<0.945	2391.3	0.00206	0.377
300-500	2.7	139.5	<0.945	1041.3	0.00129	0.377
500-800	5.1	110.6	<0.875	146.3	0.000223	0.210
800-1200	10.0	89.4	<0.945	118.3	0.000557	0.323
1200-1800	20.7	78.5	<1.015	55.5	0.000391	0.319
1800-3120	57.1	6.0	<1.435	3	0.000632	0.0492
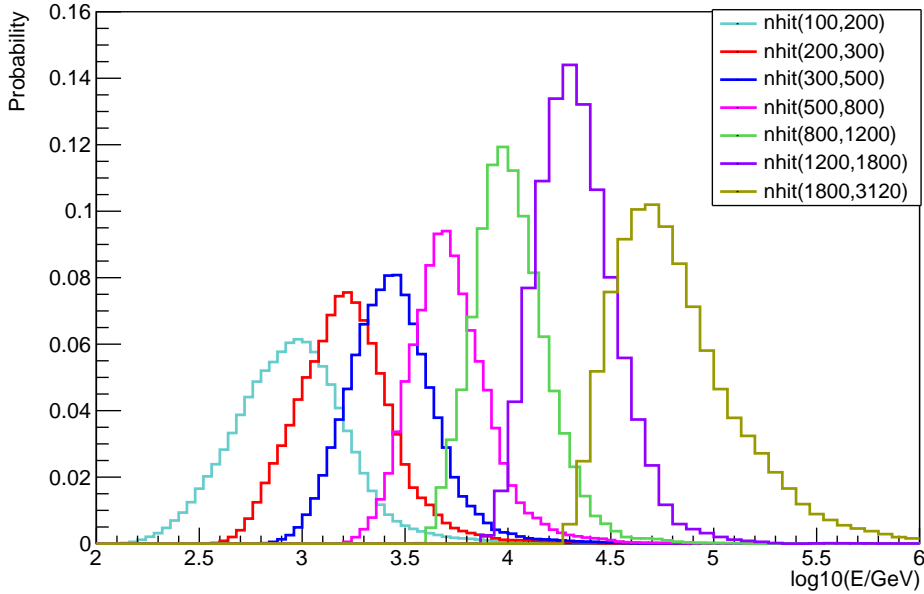
Figure 3: Normalized distributions of primary energy of gamma-ray showers from a source with a spectral index of -2.62. The color scheme for the curves is illustrated in the legend in the figure, corresponding to the seven bins.

Besides, in order to initially select cosmic ray electron events of interest, the following criteria were applied:

- $100 < N_{\text{hit}} < 1800$;

- events with a zenith angle greater than 50 degrees were excluded;

- the core position of the event is required to fall within a circle of 120m radius centered at the array center.

In consideration of the differences between hadronic and electromagnetic showers, which is reflected in the transverse spread of the shower, we are interested in electromagnetic shower events and applied the effective discrimination parameter called PINCness (Parameter for Identifying Nuclear Cosmic-rays), *P*, constructed by HAWC Collaboration [2] as a preliminary selection criterion. The PINCness parameter is defined as

$$P = \frac{1}{N} \sum_{i=0}^{N} \frac{(\zeta_i - \langle \zeta_i \rangle)^2}{\sigma_{\zeta_i}{}^2},\tag{1}$$

where $\zeta_i = \log_{10}(Q_i)$, Q_i is the hit charge, σ_{ζ_i} is the width of the distribution obtained from simulated gamma data or a sample of gamma-like events at different distances from the shower core. We evaluated the effectiveness of the PINCness condition with equal zenith angle method across various energy bins by analyzing four months of data from April 2021 to July 2021 of three pools of WCDA. Different PINCness conditions are applied for different energy ranges, and we select the PINCness condition that maximizes the significance of the crab signal. The result is shown in table1. The retention ratio of gamma-ray events and cosmic-ray events is calculated after PINCness condition selection. We also list retention ratios in the table1. Under the current selection criteria, the statistical sample consists of 1 million events at TeV, with approximately 2,000 of them being cosmic ray events.
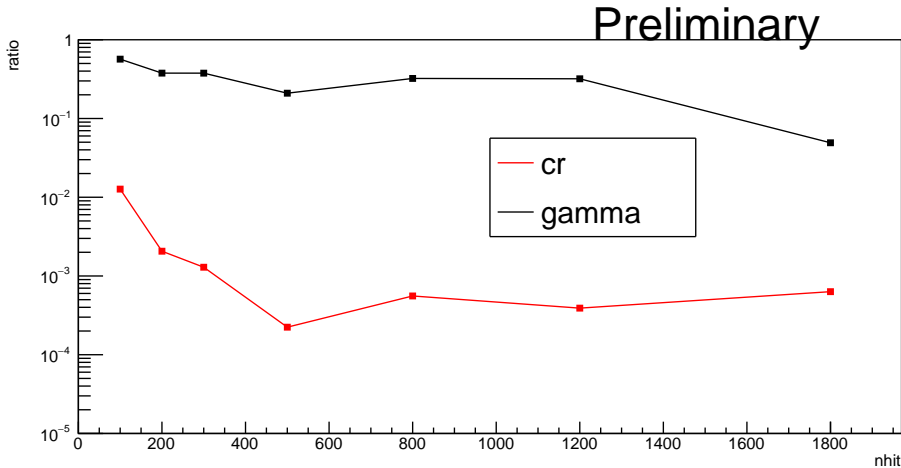
Figure 4: Retention ratio of gamma-ray events (black dot) and cosmic-ray events (red dot) after PINCness condition selection.

4. Analysis method

Anisotropic modulation can be analyzed in two time periods - local solar time and local sidereal time - based on the characteristics of anisotropy. In the experiment, the anisotropic signal is essentially the variation of the event rate in different directions in the sky. However, atmospheric effects can impact the detector efficiency and, consequently, the observed cosmic ray event rate. In this study, we use the equal zenith angle method in the all-sky fitting method to estimate the background and analyze the relative intensity of the anisotropy that is not affected by atmospheric effects, while retaining anisotropy information.

By dividing the zenith angle into 50 rings with a bin size of 1°, and each ring further into n_θ windows based on equal solid angle principle, it can be assumed that the background of each on-window and off-window on the same ring is equal. Based on this assumption, we can use the least-squares method to construct the χ^2 formula, which is given by:

$$\chi^2 = \frac{\left(\frac{N_{\mathrm{on}}}{I_{\mathrm{on}}} - \frac{1}{n_\theta} \sum_{\phi'=1}^{n_\theta} \frac{N_{\mathrm{off},\phi'}}{I_{\mathrm{off},\phi'}} \right)^2}{\sigma^2} \tag{2}$$

where the statistical error $\sigma^2 = \sigma_{\mathrm{on}}{}^2 + \sigma_{\mathrm{off}}{}^2$ in the denominator can be obtained using the error propagation formula. This formula represents the extent to which the relative intensity of each grid deviates from isotropy. The significance of each grid is calculated with the Li-Ma formula [14]:

$$S_{ij} = \frac{I_{ij} - 1}{\Delta I_{ij}}. \tag{3}$$

Due to various factors that violate the assumptions of the equal zenith angle method, we correct the data for azimuth angle before iteration to ensure a uniform distribution of azimuth angles for the same zenith angle. Additionally, as the detection efficiency of the ground array is dependent on zenith angle, the relative intensity of the declination direction cannot be absolutely calibrated. To address this issue, we performed declination normalization during the solving process by constraining the average relative intensity of part of sky regions within the same declination band to be equal to 1. This constraint enabled us to obtain a unique solution. Finally, we smoothed the results of the iteration using a 15°top hat function to smooth and masked the Galactic plane within a range of ±6°.

5. Summary

We endeavored to analyze the anisotropy of CREs using two years' selected data from three pools of WCDA. Preliminary skymaps are generated at two energy bin, which uncovered a challenge in analyzing CREs due to inadequately pure samples. This is a challenge that we aim to tackle in our future research. In the meanwhile, careful and detailed study of more refined gamma ray source subtraction is essential to obtain accurate results.

6. Acknowledgments

References

[1] Abdollahi, S., Ackermann, M., Ajello, M., et al. 2017, Phys. Rev. Lett. , 118, 091103, doi: 10.1103/PhysRevLett.118.091103

[2] Abeysekara, A. U., Albert, A., Alfaro, R., et al. 2017, Astrophys. J. , 843, 39, doi: 10.3847/1538-4357/aa7555

[3] Ackermann, M., Ajello, M., Atwood, W. B., et al. 2010, Phys. Rev. D , 82, 092003, doi: 10.1103/PhysRevD.82.092003

[4] Adriani, O., Barbarino, G. C., Bazilevskaya, G. A., et al. 2011, Science, 332, 69, doi: 10.1126/science.1199172

[5] Aguilar, M., Aisa, D., Alpat, B., et al. 2015, Phys. Rev. Lett. , 114, 171103, doi: 10.1103/PhysRevLett.114.171103

[6] Aharonian, F., An, Q., Axikegu, et al. 2021, Chinese Physics C, 45, 085002, doi: 10.1088/1674-1137/ac041b

[7] Ahn, H. S., Allison, P. S., Bagliesi, M. G., et al. 2010, Astrophys. J. , 715, 1400, doi: 10.1088/0004-637X/715/2/1400

[8] Bernard, G., Delahaye, T., Salati, P., & Taillet, R. 2012, Astron. Astrophys. , 544, A92, doi: 10.1051/0004-6361/201219502

[9] Cao, Z., della Volpe, D., Liu, S., et al. 2019, arXiv e-prints, arXiv:1905.02773, doi: 10.48550/arXiv.1905.02773

[10] DAMPE Collaboration, Ambrosi, G., An, Q., et al. 2017, Nature , 552, 63, doi: 10.1038/nature24475

[11] Fang, K., Bi, X.-J., Yin, P.-F., & Yuan, Q. 2018, Astrophys. J. , 863, 30, doi: 10.3847/1538-4357/aad092

[12] Gaensler, B. M., & Slane, P. O. 2006, Annu. Rev. Astron. Astrophys., 44, 17

[13] Kirk, J. G., Lyubarsky, Y., & Petri, J. 2009, in Astrophysics and Space Science Library, Vol. 357, Astrophysics and Space Science Library, ed. W. Becker, 421, doi: 10.1007/978-3-540-76965-1_16

[14] Li, T. P., & Ma, Y. Q. 1983, Astrophys. J. , 272, 317, doi: 10.1086/161295

[15] Liu, W., Guo, Y.-Q., & Yuan, Q. 2019, J. Cosmol. Astropart. Phys. , 2019, 010, doi: 10.1088/1475-7516/2019/10/010

[16] Luo, Q., Qiao, B.-Q., Liu, W., Cui, S.-W., & Guo, Y.-Q. 2022, Astrophys. J. , 930, 82, doi: 10.3847/1538-4357/ac6267

[17] Mertsch, P. 2011, J. Cosmol. Astropart. Phys. , 2011, 031, doi: 10.1088/1475-7516/2011/02/031

[18] Panov, A. D., Adams, J. H., Ahn, H. S., et al. 2006, arXiv e-prints, astro, doi: 10.48550/arXiv.astro-ph/0612377

[19] —. 2009, Bulletin of the Russian Academy of Sciences, Physics, 73, 564, doi: 10.3103/S1062873809050098

[20] Qiao, B.-Q., Liu, W., Guo, Y.-Q., & Yuan, Q. 2019, J. Cosmol. Astropart. Phys. , 2019, 007, doi: 10.1088/1475-7516/2019/12/007

[21] Serpico, P. D. 2012, Astroparticle Physics, 39, 2, doi: 10.1016/j.astropartphys.2011.08.007

[22] Yoon, Y. S., Ahn, H. S., Allison, P. S., et al. 2011, Astrophys. J. , 728, 122, doi: 10.1088/0004-637X/728/2/122